

Prediction of a Novel 2D Porous Boron Nitride Material with Excellent Electronic, Optical and Catalytic Properties

Vikram Mahamiya^a, Alok Shukla^{a}, and Brahmananda Chakraborty^{b,c}*

^aIndian Institute of Technology Bombay, Mumbai 400076, India

^bHigh pressure and Synchrotron Radiation Physics Division, Bhabha Atomic Research Centre, Bombay, Mumbai, India-40085

^cHomi Bhabha National Institute, Mumbai, India-400094

email: mahamiyavikram@gmail.com ; shukla@iitb.ac.in ; brahma@barc.gov.in

ABSTRACT

Holey graphyne (HGY) is a recently synthesized two-dimensional semiconducting allotrope of carbon composed of a regular pattern of six and eight-vertex carbon rings. In this study, based on first-principles density functional theory and molecular dynamics simulations, we predict a similar stable porous boron nitride holey graphyne-like structure that we call BN-holey-graphyne (BN-HGY). The dynamical and thermal stability of the structure at room temperature is confirmed by performing calculations of the phonon dispersion relations, and also *ab-initio* molecular dynamics simulations. BN-HGY structure has a wide direct bandgap of 5.18 eV, which can be controllably tuned by substituting carbon, aluminum, silicon, and phosphorus atom in place of sp and sp² hybridized boron and nitrogen atoms of BN-HGY. We have also calculated the optical properties of the HGY and BN-HGY structures for the first time and found that the optical absorption spectra of these structures span full visible and a wide range of ultraviolet regions. We found that the Gibbs free energy of the BN-HGY structure for the

hydrogen adsorption process is very close to zero (-0.04 eV) and, therefore, the BN-HGY structure can be utilized as a potential catalyst for HER. Therefore, we propose that the boron nitride analog of holey graphyne can be synthesized, and it has a wide range of applications in nanoelectronics, optoelectronics, spintronics, ultraviolet laser, and solar cell devices.

Keywords: Holey graphyne, Density functional theory, Boron nitride, 2D material, Molecular dynamics

1. INTRODUCTION

Carbon nanomaterials have received a lot of scientific interest due to the ability of carbon to get hybridized in sp^3 , sp^2 , and sp form and making various stable allotropes, with unique electronic properties¹⁻⁴. The experimentally synthesized carbon allotropes of various dimensions, including fullerenes⁵, carbon nanotubes⁶, graphene⁷ etc. have been explored widely. Pristine graphene has zero energy bandgap that limits its applications in the operation of electronic and optoelectronic devices. Therefore, a lot of scientific research has been carried out for the bandgap opening of graphene and synthesizing other 2D materials with suitable bandgaps. There has been extensive study to open the bandgap of graphene by using defects, doping, external electric field, strain, changing the stacking nature, etc.⁸⁻¹⁵. In addition to that, there are some other semiconducting nanostructures, including transition metal dichalcogenides (MX_2 , where $M = Mo, W$; $X = S, Se$)¹⁶⁻²⁰, Mxenes²¹⁻²⁴, hexagonal boron nitrides (h-BN)^{25,26}, etc., that have been thoroughly explored due to their applications in electronics, photonics, and optoelectronics. Graphyne family structures which were formed by benzene rings and acetylene linkage have gained enormous scientific interest due to their large holes, which can be utilized for energy storage purposes²⁷⁻²⁹. By increasing the length of the acetylene linkage in graphyne structures, the electronic bandgap can be tuned, and it was found

that the graphyne family has exceptional electronic³⁰, optical³¹, and mechanical properties³². Furthermore, the carrier mobility in graphyne is even more than graphene³³.

After the experimental synthesis of graphyne structures in 2017^{34,35}, their electronic, optoelectronic, and spintronic properties have been widely explored. The graphyne family structures are utilized as anodes for battery applications^{36–38}, transistors^{39,40}, gas sensing^{41–44}, hydrogen evolution reaction and storage^{45–50}, etc. Wang *et al.*⁵¹ have synthesized boron-graphdiyne structure and explored its application for Na ion storage. Ding *et al.*⁵² have recently synthesized N-graphyne structure by one-step ball milling of CaC₂ and pyrazine. They have reported that N-graphyne has potential applications in electrocatalysis and supercapacitor. The graphitic carbon g-C₃N₄ is another two dimension structure which has been thoroughly explored after its experimental realization^{53,54}. The nitrogenated holey graphene (C₂N) structure has also been synthesized and explored for field-effect transistor applications by Mahmood *et al.*⁵⁵. The experimental synthesis of these carbon-boron and carbon-nitrogen structures has opened the door towards post-silicon nanoelectronics. The controlled introduction of boron and nitrogen atoms into carbon nanostructures can tune their electronic and chemical properties. The BN is isoelectronic to CC, having a similar bond length but very different electronic properties. The BN analogs of carbon nanostructures have a wide bandgap and have potential applications in nanoelectronics device fabrication^{56–59}. The two-dimensional BN sheets, BN analog of graphyne BN-yne and BN nanoribbons have been synthesized and theoretically studied^{60–62}. The BN analog of two-dimensional porous triphenylene graphdiyne (TpG) has also been theoretically explored by Muhammad *et al.*⁶³.

Very recently, a new two-dimensional porous carbon structure with a periodic pattern of six and eight-vertex rings, holey graphyne (HGY), has been successfully synthesized⁶⁴. Liu *et al.*⁶⁴ have reported that HGY is a p-type semiconductor with high electron and hole mobility at room temperature. The HGY structure has uniform periodic holes, which can be utilized for energy

storage applications. Hydrogen storage in Li and Sc decorated HGY structures have been explored by Guo *et al.*⁶⁵ and Mahamiya *et al.*⁶⁶, respectively.

In this paper, we have explored the possibility of synthesizing BN analog of two-dimensional HGY by theoretically investigating its stability and various properties suitable for different applications. We found that the BN analog of HGY structure is energetically and dynamically stable. We have also observed that the bandgap of the BN-HGY structure can be tuned, and that the optical absorption of HGY and BN-HGY span a wide range of visible and ultraviolet regions. In addition to that, the BN-HGY structure exhibit excellent catalytic activity towards hydrogen evolution reaction (HER). Hence, the proposed BN-HGY system has potential applications in nanoelectronics, optoelectronics, solar cells, and hydrogen production.

2. COMPUTATIONAL DETAILS

We have performed the density functional theory (DFT) and *ab-initio* molecular dynamics (AIMD) calculations using the Vienna *ab-initio* simulation package (VASP)^{67–70}. The generalized gradient approximation (GGA) with Perdew-Burke-Ernzerhof (PBE) exchange-correlation functional was used for the calculations⁷¹. We have taken a vacuum space of 20 Å along the z-direction to avoid the periodic interaction between two consecutive layers. A Monkhorst-pack K-point grid $5 \times 5 \times 1$ was taken to sample the Brillouin zone, and convergence limits of 0.01 eV/Å and 10^{-5} eV were considered for the force and total energy optimization, respectively. A Monkhorst-pack grid of $7 \times 7 \times 1$ kpoints was taken to calculate the electron localization function (ELF)⁷² for the BN-HGY structure. The ELF can explain the qualitative distribution of electron density and the nature of chemical bonds present in this novel material. The values of ELF ranges between zero to one, corresponding to a region of very low electron density to high electron density for localized electrons, respectively. The phonon dispersion

calculations were performed using density functional perturbation theory method. We have checked the stability of the structure at room temperature by performing the *ab-initio* molecular dynamics (AIMD) simulations. AIMD simulations solve electronic Schrodinger equations for the nuclei at each time step and compute the potential energy surfaces. Thus a lot of crucial information, such as charge transfer, bond dissociation and formation, change in electronic states^{73,74}, etc., can be obtained by performing AIMD simulations which are difficult to find out from the classical MD based on empirical force fields. However, AIMD simulations are very costly since each time step involves a single DFT energy and force calculations, so trajectories are limited to picoseconds of simulation time, and the general time step should be of the order of femtoseconds to ensure numerical stability.⁷⁵ The AIMD simulations are performed in two consecutive steps, initially, we put the relaxed structure of BN-HGY in a microcanonical ensemble (NVE) for 5 ps time and the temperature of the system is increased up to 300 K in a time step of 1 fs. Next, we kept this structure in a canonical ensemble (NVT) at 300 K by employing the Nose–Hoover thermostat⁷⁶ for another 5 ps time duration. We have also investigated the thermal stability of the BN-HGY structure at a high temperature of 1000 K by following the same procedure.

3. RESULTS AND DISCUSSION

3.1 Structural stability

The final optimized structures of the $2 \times 2 \times 1$ supercell of HGY and BN-HGY are shown in **Fig. 1 (a & b)**. The lattice constants for the hexagonal BN-HGY structure are $a = b = 10.92 \text{ \AA}$, which are close to the pristine HGY lattice constants value of 10.85 \AA ⁶⁵. There are four different values of BN bond lengths corresponding to sp^2 - sp^2 , sp^2 - sp , and sp - sp hybridized boron and nitrogen atoms, as shown in **Fig. 1 (b)**. C1, B1, and N1 denote sp -hybridized carbon, boron,

and nitrogen atoms, while C2, B2, and N2 denote sp^2 -hybridized carbon, boron, and nitrogen atoms, as displayed in **Fig. 1 (a & b)**.

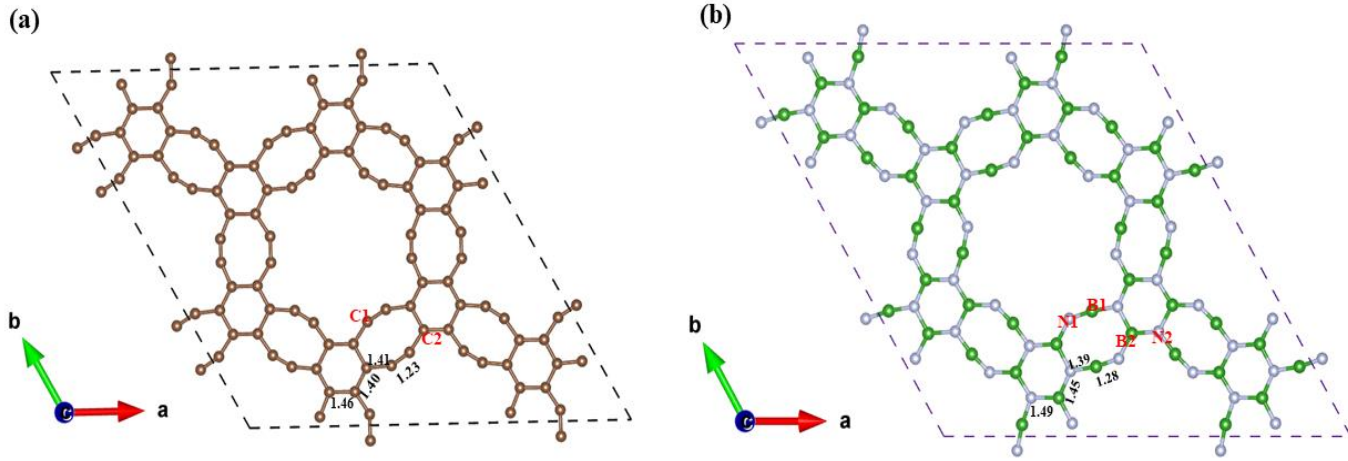


Fig. 1 Optimized structure of (a) $2\times 2\times 1$ supercell of HGY. (b) $2\times 2\times 1$ supercell of BN-HGY. Here C1, B1 and N1 represent sp -hybridized carbon, boron and nitrogen atoms, while C2, B2 and N2 represent sp^2 hybridized carbon, boron and nitrogen atoms, respectively.

The BN-HGY structure has two sp^2 - sp^2 hybridized bonds with bond lengths 1.49 and 1.45 Å, and one each sp^2 - sp and sp - sp hybridized bond with bond lengths 1.39 and 1.28 Å, respectively. Since BN and CC are isoelectronic and the boron and nitrogen atoms are located on sites similar to those of the carbon atoms in HGY, the change in the bond lengths of the BN analog of HGY compared to HGY is small. The change in the CC and BN bond length arises because the atomic radii and the electronegativities of boron and nitrogen atoms are different as compared to the carbon atoms. The angle between the hexagon of BN-HGY and acetylene linkage is 125.1° , which is close to the corresponding bond angle 126.03° in HGY, and larger than the bond angle 120° for graphyne. A detailed comparison of the structural parameters of HGY and BN-HGY is presented in **Table 1**.

Table 1. The structural parameters of HGY and BN-HGY.

Structural parameter	Bond lengths (Å)			Bond angle (degree)
	$sp^2 - sp^2$	$sp^2 - sp$	$sp - sp$	
HGY	1.46, 1.40	1.41	1.23	126.03
BN-HGY	1.49, 1.45	1.39	1.28	125.10

We have investigated the stability of the BN-HGY structure by calculating its cohesive and per-atom energy. We have also calculated the cohesive and per-atom energy of some stable BN analogs including, the BN analog of graphene and BN analog of carbon nanotube, to compare with the BN-HGY structure and investigated the feasibility of its synthesis. The cohesive energy of the BN-HGY structure is found to be -6.52 eV which is very close to the cohesive energy of the HGY structure -6.76 eV calculated at the same level of theory. Shin *et al.*⁷⁷ have found that the cohesive energy of the most stable graphyne form γ -graphyne is -6.76 eV, very similar to HGY and BN-HGY structures. The cohesive energy of monolayer MoS₂ is -4.98 eV⁷⁸ lesser than the cohesive energy of BN-HGY. We have found that the cohesive energies of the BN analogs of graphene and carbon nanotube are found to be -7.12 eV and -6.96 eV, respectively. Further, we have also calculated that the per-atom energy of the BN-HGY structure -8.21 eV, which is also very close to the per-atom energy of the HGY structure, -8.46 eV. The per-atom total energies of the BN analogs of graphene and carbon nanotube are found to be -8.81 eV and -8.66 eV, respectively. The cohesive and per-atom energies of the BN analog of HGY are very close to those quantities of the pristine HGY and other stable BN analog

structures, suggesting that the experimental realization of the BN-HGY structure is energetically feasible.

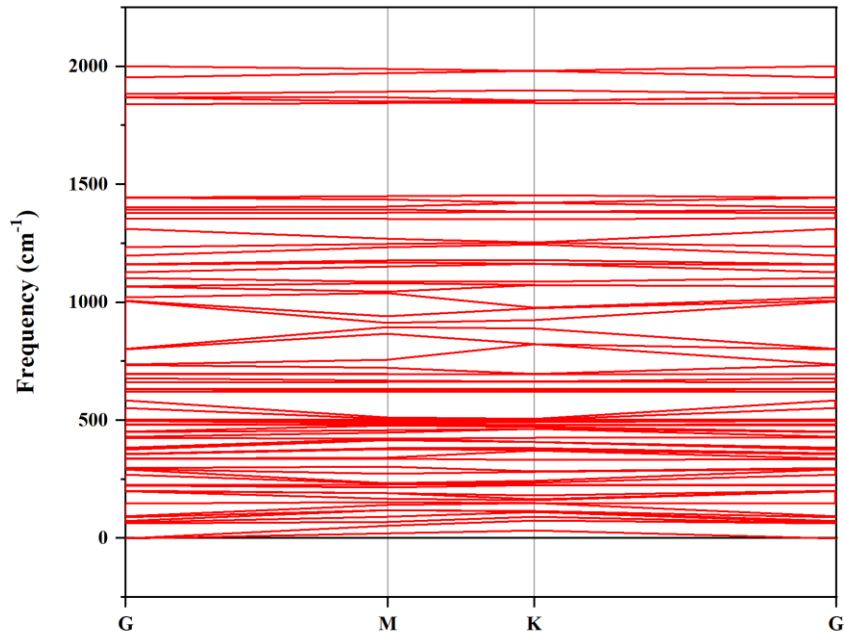


Fig. 2 Calculated phonon dispersion relations of BN-HGY.

The phonon dispersion curve of the BN-HGY presented in **Fig. 2**, contains only real frequencies in the full Brillouin zone, indicating that the BN-HGY structure is dynamically stable.

3.2 Thermal stability

To check the thermal stability of the structure at room temperature and also at high temperatures, we have performed *ab-initio* molecular dynamics simulations. The molecular dynamics snapshot of the BN-HGY after keeping it in a canonical ensemble for 5 picoseconds at room temperature is shown in **Fig. 3(a)**. The thermal fluctuations around room temperature are small, as shown in **Fig. 3(b)**. We found that the structure does not deform at room temperature and the changes in the B-N bond lengths are negligible. The bond length fluctuations of the sp-sp, sp-sp², and sp²-sp² B-N bonds are small at room temperature, as shown in **Fig. 4(a)**. We have observed that the maximum fluctuations for sp-sp, sp-sp², and sp²-sp² bonds are 3.9 %, 7.7 %, and 6.2 % of their mean values, respectively, at room temperature. Although the maximum fluctuations in B-N bonds increase up to ~ 20 % at a high temperature of 1000 K, as shown in **Fig. 4(b)**, the B-N bonds do not break, and the structure is intact.

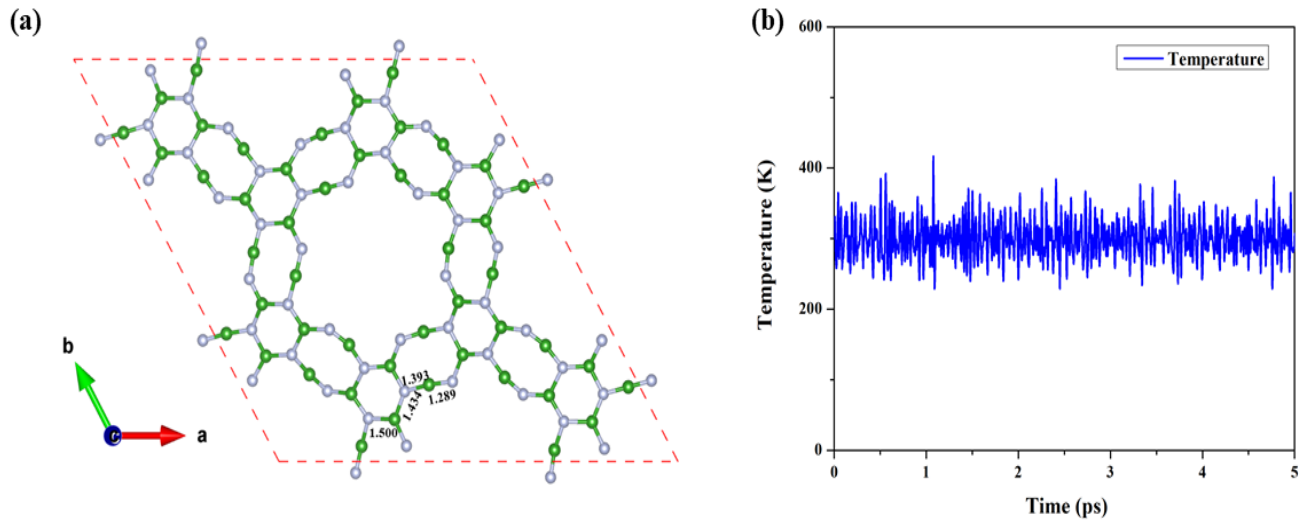


Fig.3 (a) Molecular dynamics snapshot of BN-HGY. (b) Fluctuations of temperature around room temperature.

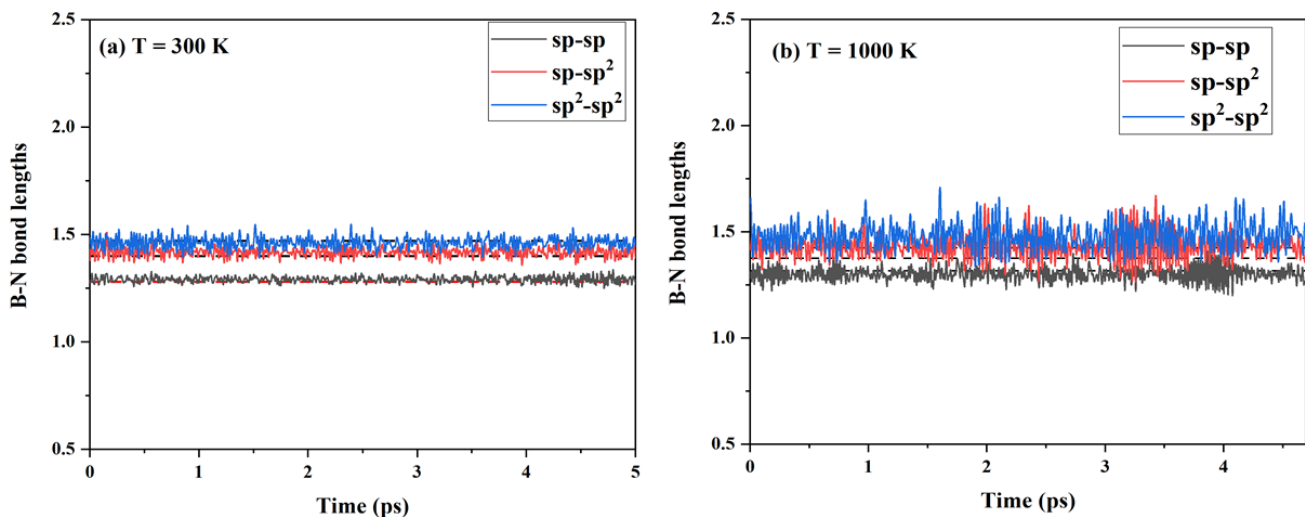


Fig. 4 Fluctuations in sp-sp, sp-sp², and sp²-sp² hybridized B-N bond lengths at (a) 300 K, (b) 1000 K, after keeping the system in a canonical ensemble for 5 ps time duration.

The molecular dynamics snapshot and structural coordinates of BN-HGY, after putting the structure in a canonical ensemble for 5 picoseconds time duration at 1000 K, are provided in the supporting information file (See **Fig. S1**). The B-N bonding in the two-dimensional BN-HGY structure is very strong due to which BN-HGY material can withstand up to high temperatures. Previously, Muhammad *et al.*⁶³ have reported the BN-analog of two-dimensional triphenylene-graphdiyne is stable up to 1500 K, and the structure breaks at around 2000 K by performing AIMD simulations for 5 ps in the time step of 1 fs. The thermal fluctuations in the BN-HGY structure, after keeping the system in a canonical ensemble at 1000 K for 5 ps time are moderate, as presented in **Fig. S2** of the supporting information file.

3.3 Electronic properties

The total density of states of HGY and BN-HGY structures are shown in **Fig. 5**. The pristine HGY structure has a direct bandgap of 0.4 eV when calculated using PBE exchange-correlation functional, which is in excellent agreement with the literature.^{79,80}

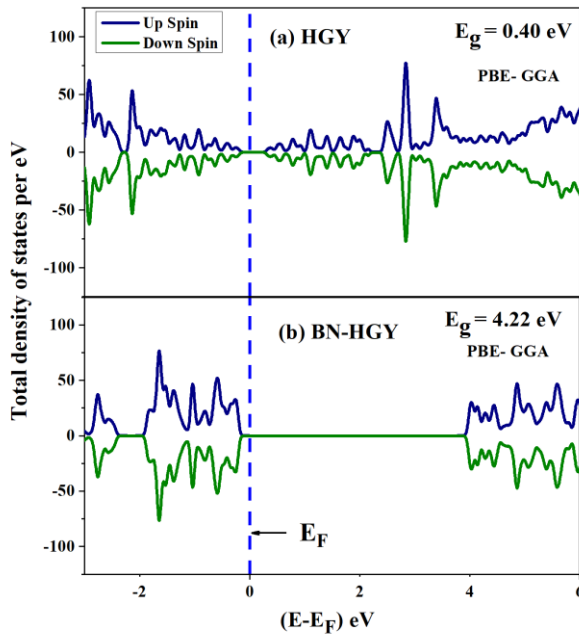


Fig. 5 Total density of states of (a) Monolayer holey graphyne (b) Boron nitride analog of monolayer holey graphyne. E_F represents the Fermi level.

On the other hand, using the same functional, the band gap of BN-HGY also turns out to be direct, but with the value 4.22 eV, which is comparatively much larger than that of HGY. Since PBE exchange-correlation underestimates the band gap, we have also calculated the band gap of HGY and BN-HGY structures by employing HSE06⁸¹ functional. We found that the band gap of the HGY structure is 0.9 eV using HSE06 functional, excellently matching with the experimental value of 1 eV⁷⁹. Here, we report 5.18 eV of band gap for BN-HGY structure using HSE06 exchange-correlation. BN analog of graphene and graphyne (BN-yne) are also direct band gap materials with band gaps 4.64 eV and 2.65 eV, respectively, computed using the PBE exchange-correlation^{61,82}. Since nitrogen atom is more electronegative compared to boron,

nitrogen and boron atoms are connected by strongly polarized covalent bond, due to which the BN structures are wide bandgap materials. The total density of states of the HGY and BN-HGY structure is symmetric for the upper and lower panels, as shown in **Fig. 5**, which explains the non-magnetic nature of these structures. Since the HGY and BN-HGY structures have sp and sp²–hybridized carbon, boron and nitrogen atoms, we have plotted the partial density of states (PDOS) of the 2p-orbitals of carbon, boron, and nitrogen atoms as displayed in **Fig. 6 (a & b)**.

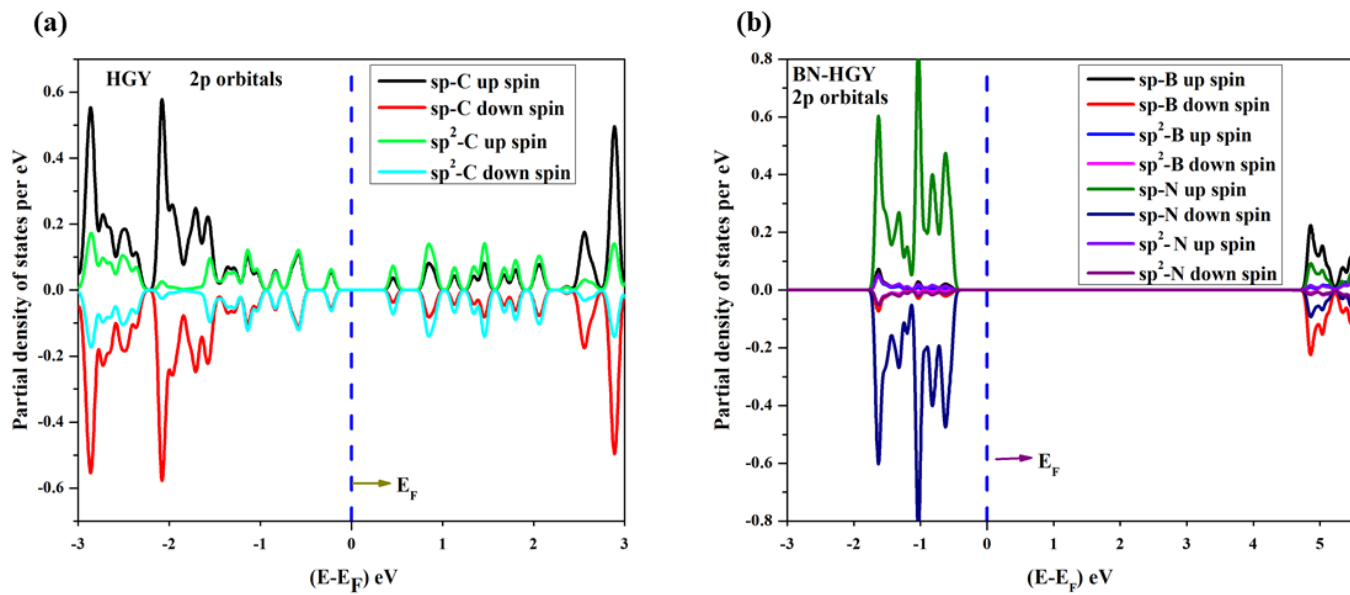


Fig. 6 Partial density of states of 2p-orbitals of the (a) sp and sp²-hybridized carbon atoms of holey graphyne (b) sp and sp²-hybridized boron and nitrogen atoms of the boron nitride analog of monolayer holey graphyne. E_F represents the Fermi level.

The total density of states of the HGY structure is dominated by the PDOS of the 2p-orbitals of carbon atoms. We have observed more intense states for sp-hybridized carbon atoms compared to sp²-hybridized carbon in HGY. The total density of states of BN-HGY structure is mainly contributed by the 2p-orbitals of the sp-hybridized nitrogen atoms. The sp-hybridized bond is more electronegative due to more contribution of s-orbitals as compared to sp²-hybridization. This is the reason behind the intense peaks of the sp-hybridized carbon and

nitrogen atoms in the 2p-orbitals PDOS of HGY and BN-HGY. We have plotted the detailed band structures of HGY and BN-HGY along the G-M-K-G high symmetry path, as shown in **Fig. 7**, and report that the BN-HGY structure is a direct band gap material.

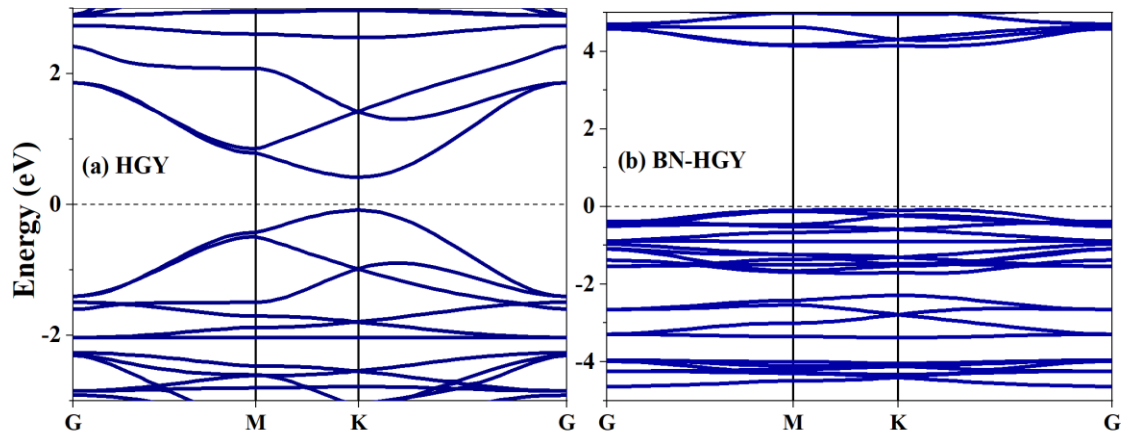


Fig. 7 Band structure plots of (a) Monolayer holey graphyne (b) Boron nitride analog of holey graphyne.

To further investigate the electronic properties of the BN-HGY structure, we have plotted the charge density plot for an isosurface value of 0.133e, as shown in **Fig. 8 (a)**. The yellow color region around the nitrogen atoms denotes the charge accumulation region. We have also plotted the ELF for the accurate investigation of charge distribution in this material, as displayed in **Fig 8 (b)**. The red color region of **Fig. 8 (b)** denotes the charge gain region where electrons are localized. We found that the electrons are localized around the nitrogen atoms of BN-HGY due to their high electronegativity compared to boron atoms. As electronic charge is accumulated around the nitrogen atoms, the covalent B-N bonds in this structure get polarized.

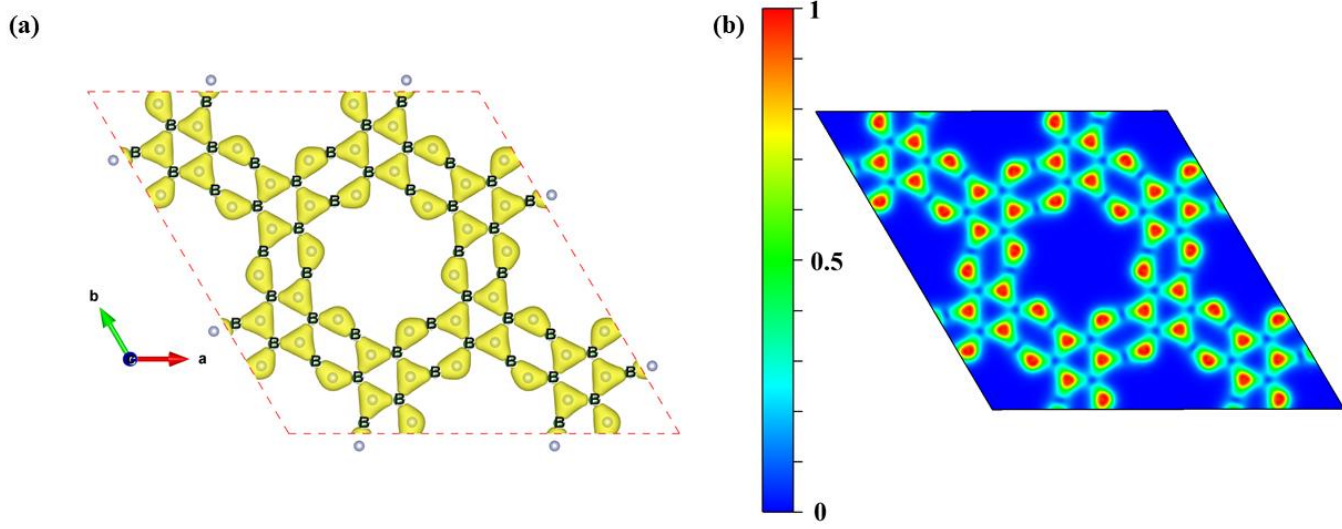


Fig. 8 (a) Charge density plot of the BN-HGY structure. Here, yellow colored region around the nitrogen atoms denotes the charge accumulation region. (b) Electron localization function plot for the BN-HGY structure. Here, red colored region around the nitrogen atoms denotes the charge rich region.

3.4 Bandgap engineering

Next, we have investigated the bandgap modulation in the BN analog of the HGY structure by substituting carbon (C), aluminum (Al), silicon (Si), and phosphorus (P) atoms in place of boron and nitrogen atoms and found that the electronic bandgap of the BN-HGY structure can be reduced significantly by doping C at the B1, N1 (sp -hybridized) and B2, N2 (sp^2 hybridized) boron and nitrogen atoms. The total density of states of the C doped BN-HGY structures is shown in **Fig. 9**. We found that the large band gap 4.22 eV of the BN-HGY structure can be

tuned to 0.35 eV, by the doping of a single carbon atom at the sp -hybridized nitrogen atom, as shown in **Fig. 9 (c)**.

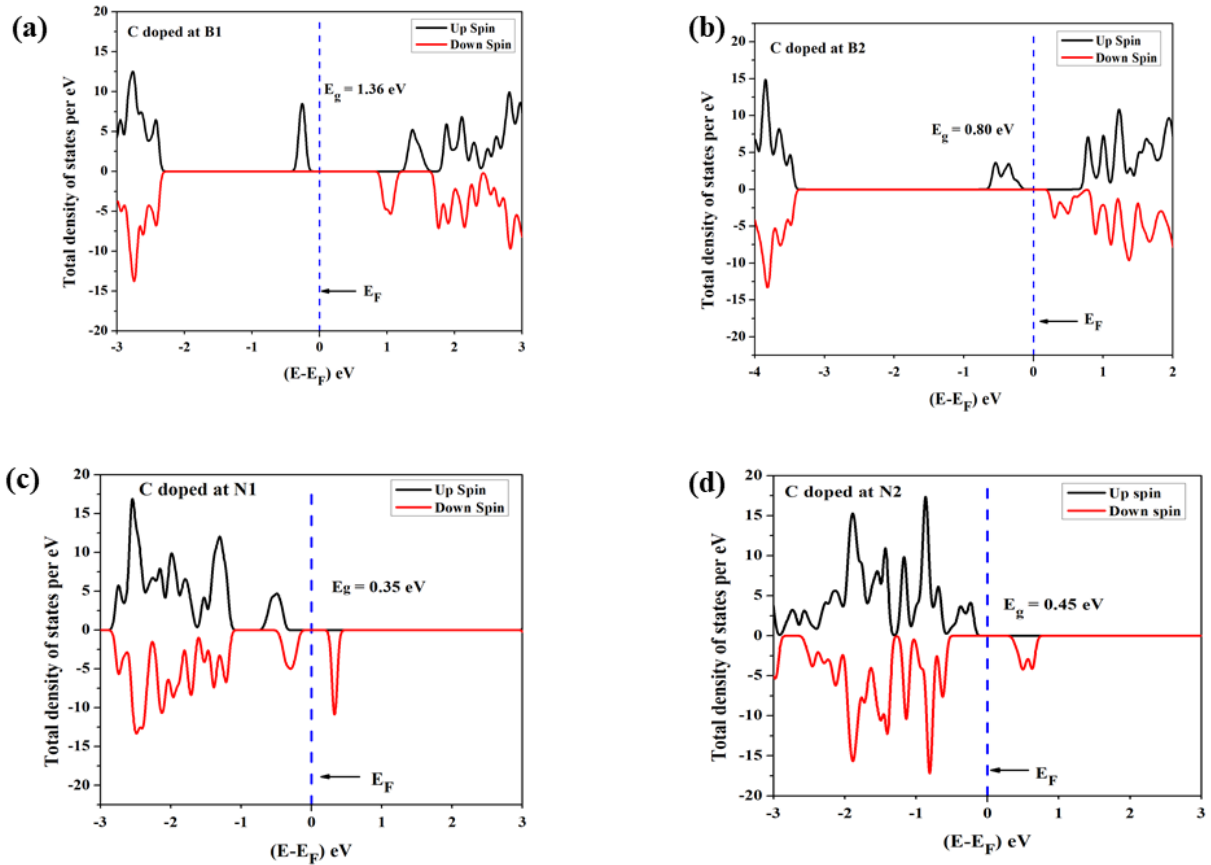


Fig. 9 Total density of states of BN-HGY with (a) Single carbon atom doped at sp -hybridized boron atom (b) Single carbon atom doped at sp^2 -hybridized boron atom (c) Single carbon atom doped at sp -hybridized nitrogen atom (d) Single carbon atom doped at sp^2 -hybridized nitrogen atom. E_F represents the Fermi level.

Further, we have substituted Al, Si, and P atoms at the sp and sp^2 hybridized boron and nitrogen atoms of the BN-HGY structure and found that the band gap of the pristine BN-HGY structure can be controllably tuned by the doping of single Al, Si, and P atoms at the sp and sp^2 -hybridized boron atoms (B1, B2). The BN-HGY structure gets distorted when Al, Si, and P atoms are placed at N1 and N2. The total density of states of the Al, Si, and P doped BN-HGY

structures are shown in **Fig. S3** of supporting information. Since the electronic band gap of the BN-HGY structure can be engineered in a controllable manner by the doping of C, Al, Si, and P atoms, the BN-HGY structure has potential applications in nanoelectronics. We have also observed that the electronic bandgap of the BN-HGY structure reduces significantly by light alkali, alkaline-earth, and transition-metal (Li, Mg, Sc, and Y) decoration, which indicates that the porous BN-HGY structure can be utilized for energy storage purposes. Further, we have found that the non-magnetic pristine BN-HGY structure becomes magnetic with the doping of C, Si, and P atoms and the decoration of Li, Sc, and Y metal atoms suggesting that the substituted BN-HGY structure can be utilized for spintronic applications. The bandgap values and induced magnetic moment of the C, Al, Si, and P doped and some metal-decorated BN-HGY structures are presented in **Table 2**.

Table 2. Tunable electronic band gaps and induced magnetic moment of the BN-HGY structure by doping of C, Si, Al, and P atoms, and decorating some light metal (Li, Mg, Sc, Y) atoms.

Structure	Electronic bandgap (eV) PBE exchange-correlation	Magnetic moment (μ_B)
Pristine BN-HGY	4.22	0.00
C doped at B1	1.36	1.00
C doped at B2	0.80	1.00
C doped at N1	0.35	1.00
C doped at N2	0.45	1.00

Al doped at B1	2.11	0.00
Al doped at B2	4.00	0.00
Si doped at B1	0.97	1.00
Si doped at B2	1.37	1.00
P doped at B1	2.37	0.00
P doped at B2	0.82	2.00
Li decorated BN-HGY	0.97	1.00
Mg decorated BN-HGY	2.44	0.00
Sc decorated BN-HGY	0.51	1.00
Y decorated BN-HGY	0.48	1.00

The total density of states for Li, Mg, Sc, and Y decorated BN-HGY structure is presented in **Fig. S4** of the supporting information.

3.5 Optical properties

In order to investigate the suitability of the HGY and BN-HGY structures for optoelectronics, we have calculated the dielectric functions, refractive indices, and absorption coefficients of these materials. To the best of our knowledge, no such previous calculations exist even for HGY. We have plotted the real and imaginary parts of the dielectric functions of monolayer HGY and BN-HGY structures with respect to energy, as shown in **Fig. 10**. The linear optical

absorption can be calculated by computing the frequency-dependent complex dielectric function $\mathcal{E}(\omega) = \mathcal{E}_1(\omega) + i \mathcal{E}_2(\omega)$, where $\mathcal{E}_1(\omega)$ and $\mathcal{E}_2(\omega)$ are its real and imaginary parts, respectively.

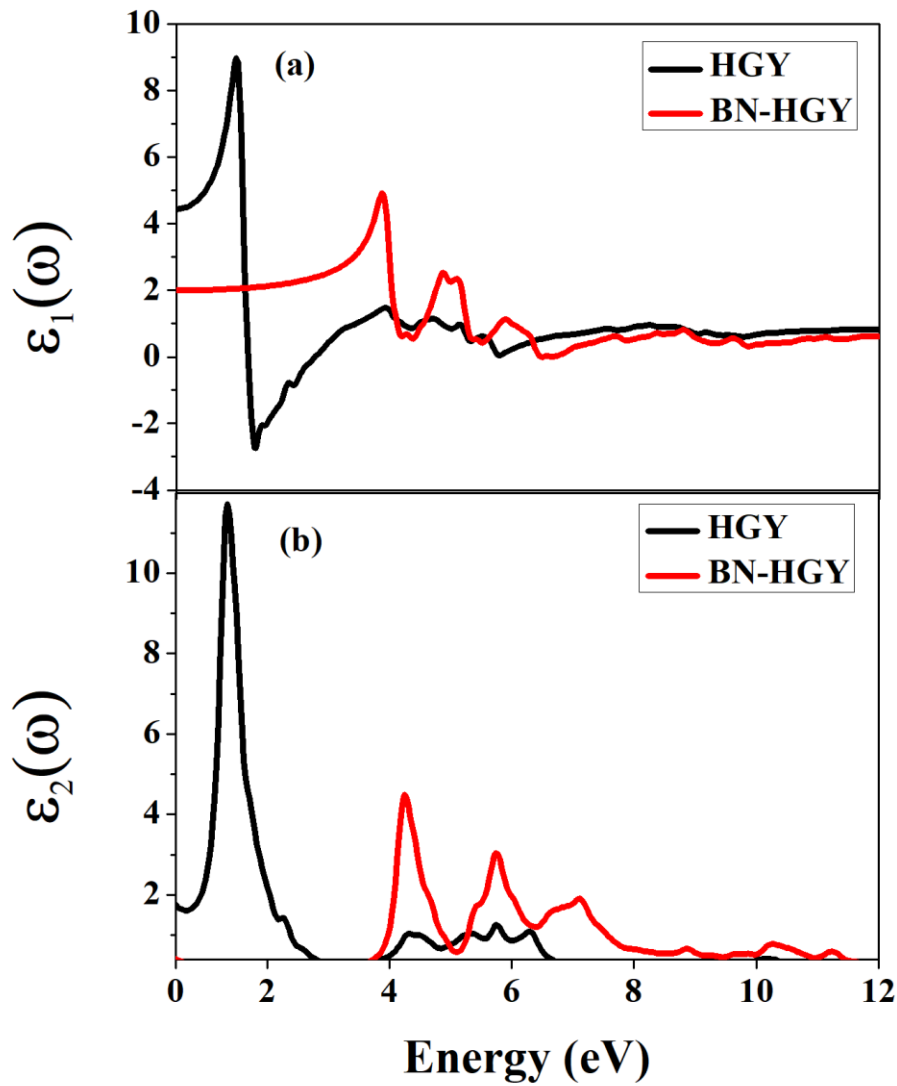


Fig. 10 Variation of the real and imaginary parts of the dielectric function of HGY and BN-HGY structure with respect to the energy of the incident photon.

The information regarding the response of a material to an incident external electromagnetic radiation of frequency ω is contained in $\epsilon(\omega)$. We have also calculated the refractive index $n(\omega)$ and absorption coefficient $\alpha(\omega)$ of these materials by using the following equations:

$$n(\omega) = \frac{1}{\sqrt{2}} \left[\sqrt{\epsilon_1^2 + \epsilon_2^2} + \epsilon_1 \right]^{\frac{1}{2}} \quad (1)$$

$$\alpha(\omega) = \sqrt{2} \omega \left[\sqrt{\epsilon_1^2 + \epsilon_2^2} - \epsilon_1 \right]^{\frac{1}{2}} \quad (2)$$

The frequency dependent linear optical absorption coefficients of the monolayer HGY and BN-HGY structures are presented in **Fig. 11**, while the refractive index $n(\omega)$ of the BN-HGY structure is presented in **Fig. S5** of the supporting information.

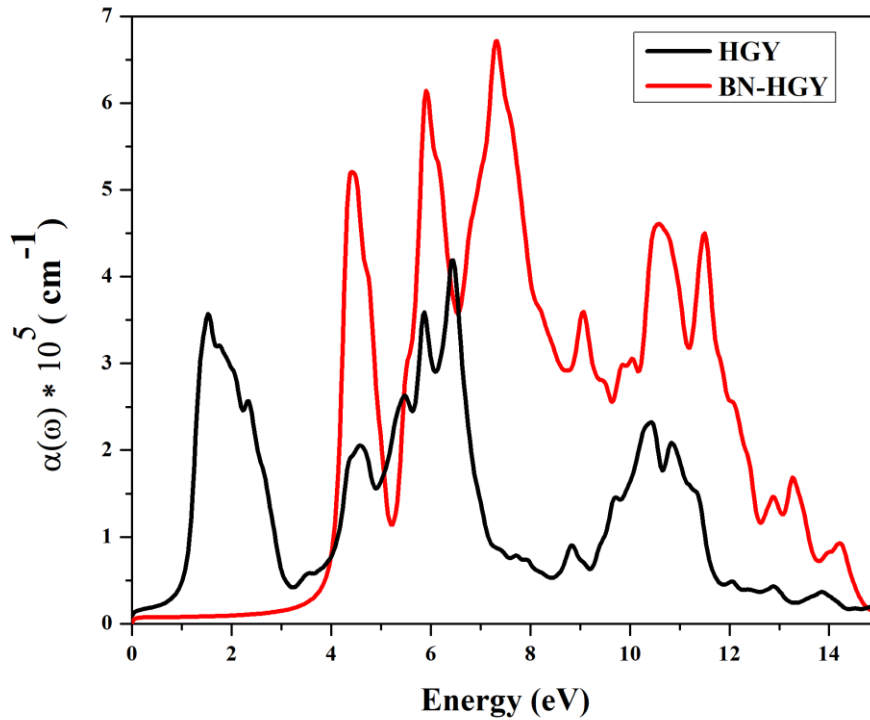


Fig. 11 Optical absorption coefficient of the HGY and BN-HGY structures, plotted with respect to the energy of the incident photon.

We have found that the linear optical absorption spectrum of HGY covers a wide range of visible and ultraviolet regions, while the optical absorption spectrum of the BN-HGY structure spans a wide range of ultraviolet region. Since the optical absorption of the HGY covers full visible region and a wide range of ultraviolet region, it will have potential applications in optoelectronics and photovoltaic solar cells. The optical absorption of the BN-HGY structure span a wide range of ultraviolet regions and it will have potential applications in ultraviolet laser devices and it can be utilized for photocatalysis and optical storage applications.

3.6 Catalytic performance for HER activity

We have also investigated the catalytic performance of the BN-HGY structure towards the hydrogen evolution reaction (HER). The HER performance of a material can be estimated by calculating its Gibbs free energy (ΔG), which is given by the following equation:

$$\Delta G = \Delta E_{ads} + \Delta E^{ZPE} - T\Delta S \quad (3)$$

Here ΔE_{ads} is the adsorption energy of the hydrogen atom on the surface of BN-HGY, ΔE^{ZPE} is the zero-point energy difference for the adsorbed hydrogen atom and isolated hydrogen in the gas phase, and $T\Delta S$ is the entropy correction term. The values of zero-point energy difference and entropy correction terms are taken from the literature^{83,84}. Catalyst with ΔG close to zero is considered suitable for HER activity due to the feasibility of the hydrogen adsorption and desorption process. We have found that the adsorption energy of hydrogen is -0.03 eV and -0.28 eV when it is kept on the top of the center of the hexagon (H) and octagon (O) sites of the BN-HGY structure, respectively. The bond length of the adsorbed hydrogen and the nearest atom of BN-HGY is 3.82 Å and 1.43 Å, when hydrogen is adsorbed at H and O sites,

respectively. We present the reaction coordinates plot for the HER activity of the BN-HGY structure in **Fig. 12**.

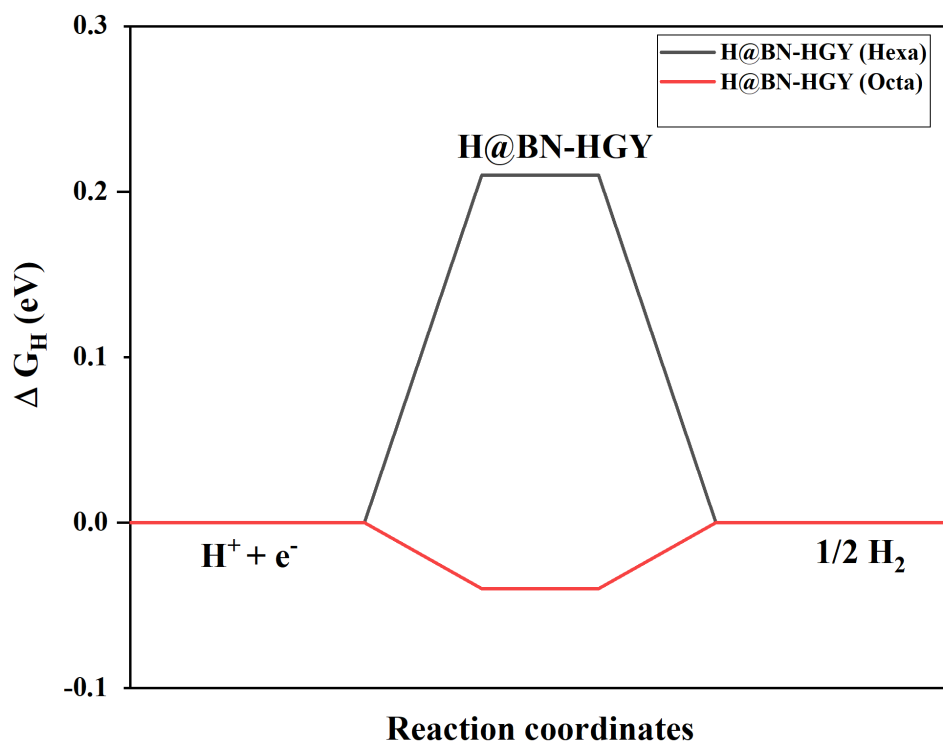


Fig. 12 Reaction coordinate plot for the HER activity of pristine BN-HGY structure.

We have found that the Gibbs free energy values of hydrogen adsorbed BN-HGY structure is 0.21 eV and -0.04 eV when hydrogen atom is attached to H and O sites, respectively which are very close to zero. Therefore, the pristine BN-HGY structure is an excellent catalyst for the HER activity.

4. CONCLUSIONS

In summary, we have theoretically predicted the novel BN-HGY structure and explored its various properties for the first time. We found that the BN-HGY structure is energetically stable, and can be realized experimentally. The dynamical and thermal stability of the BN-HGY structure is confirmed by calculating the phonon spectra and performing the *ab-initio* molecular dynamics simulations, respectively. We have observed that the BN-HGY structure is stable at room temperature and can withstand up to 1000 K. The boron nitride analog of HGY is a wide bandgap structure with a direct gap of 5.18 eV calculated using HSE06 exchange-correlation. We have found that the bandgap of the BN-HGY structure can be tuned in a controllable manner and the non-magnetic BN-HGY structure becomes magnetic with the doping of carbon, aluminum, silicon, and phosphorus atoms in place of boron and nitrogen atoms and decoration of light metal atoms, therefore, it will have potential applications in electronic and spintronic devices. The linear optical absorption spectra of pristine HGY and BN-HGY structures span a wide range of visible and ultraviolet regions, respectively, making them applicable for solar cell, ultraviolet laser, and optoelectronic device fabrication. The Gibbs free energy value for the hydrogen adsorption to the octagon site of BN-HGY is -0.04, which is very suitable for a potential catalyst for HER activity. We propose that the BN-HGY structure can be synthesized and utilized in nanoelectronics, spintronics, optoelectronics, and, catalyst for hydrogen evolution reaction.

Conflicts of Interest

There are no conflicts of interest to declare.

ACKNOWLEDGEMENTS

V. M. acknowledge Department of Science and Technology (DST), New-Delhi, for providing DST-INSPIRE fellowship. V.M. would also like to acknowledge SpaceTime-2 super-computing facility at IIT Bombay for the computing time. BC acknowledges Dr. Nandini Garg, Dr. T. Sakuntala, Dr. S.M. Yusuf and Dr. A.K. Mohanty for support and encouragement.

REFERENCES:

- 1 V. N. Mochalin, O. Shenderova, D. Ho and Y. Gogotsi, The properties and applications of nanodiamonds, *Nat. Nanotechnol.*, 2012, **7**, 11–23.
- 2 T. Braun, A. P. Schubert and R. N. Kostoff, Growth and Trends of Fullerene Research as Reflected in Its Journal Literature, *Chem. Rev.*, 2000, **100**, 23–37.
- 3 C. Wang, K. Takei, T. Takahashi and A. Javey, Carbon nanotube electronics – moving forward, *Chem. Soc. Rev.*, 2013, **42**, 2592–2609.
- 4 A. H. Castro Neto, F. Guinea, N. M. R. Peres, K. S. Novoselov and A. K. Geim, The electronic properties of graphene, *Rev. Mod. Phys.*, 2009, **81**, 109–162.
- 5 H. W. et al. Kroto, C60: Bukminsterfullerene, *Nature*, 1985, **318**, 162–163.
- 6 N. E. C. Corporation, 1-Nm Diameter, *Nature*, 1993, 603–605.
- 7 I. V. G. and A. A. F. K. S. Novoselov, A. K. Geim, S. V. Morozov, D. Jiang, Y. Zhang, S. V. Dubonos, Electric Field Effect in Atomically Thin Carbon Films, 2016, **306**, 666–669.
- 8 S. Tang, W. Wu, X. Xie, X. Li and J. Gu, Band gap opening of bilayer graphene by graphene oxide support doping, *RSC Adv.*, 2017, **7**, 9862–9871.

- 9 J. S. Park and H. J. Choi, Band-gap opening in graphene: A reverse-engineering approach, *Phys. Rev. B - Condens. Matter Mater. Phys.*, 2015, **92**, 1–12.
- 10 X. Cao, J. J. Shi, M. Zhang, X. H. Jiang, H. X. Zhong, P. Huang, Y. M. Ding and M. Wu, Band Gap Opening of Graphene by Forming Heterojunctions with the 2D Carbonitrides Nitrogenated Holey Graphene, g-C₃N₄, and g-CN: Electric Field Effect, *J. Phys. Chem. C*, 2016, **120**, 11299–11305.
- 11 S. Sahu and G. C. Rout, Band gap opening in graphene: a short theoretical study, *Int. Nano Lett.*, 2017, **7**, 81–89.
- 12 N. Ullah, R. Q. Zhang, G. Murtaza, A. Yar and A. Mahmood, Stacking nature and band gap opening of graphene: Perspective for optoelectronic applications, *Solid State Commun.*, 2016, **246**, 54–58.
- 13 M. Dvorak, W. Oswald and Z. Wu, Bandgap opening by patterning graphene, *Sci. Rep.*, 2013, **3**, 1–7.
- 14 D. Qkhoa, C. V. Nguyen, L. M. Bui, H. V. Phuc, B. D. Hoi, N. V. Hieu, V. Q. Nha, N. Huynh, L. C. Nhan and N. N. Hieu, Opening a band gap in graphene by C-C bond alternation: A tight binding approach, *Mater. Res. Express*, , DOI:10.1088/2053-1591/aaf914.
- 15 P. L. Silvestrelli and A. Ambrosetti, Bandgap opening in graphene using alkali ions by first principles, *Appl. Phys. Lett.*, , DOI:10.1063/1.5060660.
- 16 Q. H. Wang, K. Kalantar-Zadeh, A. Kis, J. N. Coleman and M. S. Strano, Electronics and optoelectronics of two-dimensional transition metal dichalcogenides, *Nat. Nanotechnol.*, 2012, **7**, 699–712.

- 17 D. Jariwala, V. K. Sangwan, L. J. Lauhon, T. J. Marks and M. C. Hersam, Emerging device applications for semiconducting two-dimensional transition metal dichalcogenides, *ACS Nano*, 2014, **8**, 1102–1120.
- 18 G. Fiori, F. Bonaccorso, G. Iannaccone, T. Palacios, D. Neumaier, A. Seabaugh, S. K. Banerjee and L. Colombo, Electronics based on two-dimensional materials, *Nat. Nanotechnol.*, 2014, **9**, 768–779.
- 19 D. Akinwande, N. Petrone and J. Hone, Two-dimensional flexible nanoelectronics, *Nat. Commun.*, , DOI:10.1038/ncomms6678.
- 20 K. F. Mak and J. Shan, Photonics and optoelectronics of 2D semiconductor transition metal dichalcogenides, *Nat. Photonics*, 2016, **10**, 216–226.
- 21 M. Khazaei, A. Ranjbar, M. Arai, T. Sasaki and S. Yunoki, Electronic properties and applications of MXenes: a theoretical review, *J. Mater. Chem. C*, 2017, **5**, 2488–2503.
- 22 Y. Xie, Y. Dall’Agnese, M. Naguib, Y. Gogotsi, M. W. Barsoum, H. L. Zhuang and P. R. C. Kent, Prediction and characterization of mxene nanosheet anodes for non-lithium-ion batteries, *ACS Nano*, 2014, **8**, 9606–9615.
- 23 Z. Xu, X. Lv, J. Chen, L. Jiang, Y. Lai and J. Li, DFT investigation of capacious, ultrafast and highly conductive hexagonal Cr₂C and V₂C monolayers as anode materials for high-performance lithium-ion batteries, *Phys. Chem. Chem. Phys.*, 2017, **19**, 7807–7819.
- 24 A. C. Rajan, A. Mishra, S. Satsangi, R. Vaish, H. Mizuseki, K. R. Lee and A. K. Singh, Machine-learning-assisted accurate band gap predictions of functionalized mxene, *Chem. Mater.*, 2018, **30**, 4031–4038.

- 25 M. P. Levendorf, C. J. Kim, L. Brown, P. Y. Huang, R. W. Havener, D. A. Muller and J. Park, Graphene and boron nitride lateral heterostructures for atomically thin circuitry, *Nature*, 2012, **488**, 627–632.
- 26 C. Pan, J. Zhang, K. Kou, Y. Zhang and G. Wu, Investigation of the through-plane thermal conductivity of polymer composites with in-plane oriented hexagonal boron nitride, *Int. J. Heat Mass Transf.*, 2018, **120**, 1–8.
- 27 Z. Jia, Y. Li, Z. Zuo, H. Liu, C. Huang and Y. Li, Synthesis and Properties of 2D Carbon - Graphdiyne, *Acc. Chem. Res.*, 2017, **50**, 2470–2478.
- 28 G. Li, Y. Li, H. Liu, Y. Guo, Y. Li and D. Zhu, Architecture of graphdiyne nanoscale films, *Chem. Commun.*, 2010, **46**, 3256–3258.
- 29 N. Narita and S. Nagai, Optimized geometries and electronic structures of graphyne and its family, *Phys. Rev. B - Condens. Matter Mater. Phys.*, 1998, **58**, 11009–11014.
- 30 K. Srinivasu and S. K. Ghosh, Graphyne and graphdiyne: Promising materials for nanoelectronics and energy storage applications, *J. Phys. Chem. C*, 2012, **116**, 5951–5956.
- 31 J. Kang, J. Li, F. Wu, S. Li and J. Xia, Elastic , Electronic , and Optical Properties of Two-Dimensional Graphyne Sheet, *J. Phys. Chem. C*, 2011, **115**, 20466–20470.
- 32 S. Kang, Z. Xiang, H. Mu and Y. Cai, Mechanical properties, lattice thermal conductivity, infrared and Raman spectrum of the fullerite C₂₄, *Phys. Lett. Sect. A Gen. At. Solid State Phys.*, 2020, **384**, 126035.
- 33 J. Chen, J. Xi, D. Wang and Z. Shuai, Carrier Mobility in Graphyne Should Be Even Larger than That in Graphene: A Theoretical Prediction, *J. Phys. Chem. Lett.*, 2013, **4**,

- 1443–1448.
- 34 Z. Jia, Z. Zuo, Y. Yi, H. Liu, D. Li, Y. Li and Y. Li, Nano Energy Low temperature , atmospheric pressure for synthesis of a new carbon Ene- yne and application in Li storage, *Nano Energy*, 2017, **33**, 343–349.
 - 35 R. Matsuoka, R. Sakamoto, K. Hoshiko, S. Sasaki, H. Masunaga, K. Nagashio and H. Nishihara, Crystalline Graphdiyne Nanosheets Produced at a Gas/Liquid or Liquid/Liquid Interface, *J. Am. Chem. Soc.*, 2017, **139**, 3145–3152 .
 - 36 H. J. Hwang, J. Koo, M. Park, N. Park, Y. Kwon and H. Lee, Multilayer Graphynes for Lithium Ion Battery Anode, *J. Phys. Chem. C*, 2013, **117**, 6919–6923.
 - 37 J. Ma, Y. Yuan, S. Wu, J. Y. Lee and B. Kang, γ -Graphyne nanotubes as promising lithium-ion battery anodes, *Appl. Surf. Sci.*, 2020, **531**, 147343.
 - 38 B. Mortazavi, M. S. I, M. E. M. I and M. Makaremi, N-, P-, As-triphenylene-graphdiyne: Strong and stable 2D semiconductors with outstanding capacities as anodes for Li-ion batteries, *Carbon*, 2019, **141**, 291-303.
 - 39 M. Hu, Y. Pan, K. Luo, J. He, D. Yu and B. Xu, Three dimensional graphdiyne polymers with tunable band gaps, *Carbon*, 2015, **91**, 518-526.
 - 40 R. Chauvin, M. A. Ratner, E. Borguet, Z. Li, M. Smeu and A. Rives, Towards graphyne molecular electronics, *Nat. Commun.*, 2015, 6, 6321.
 - 41 P. Zhang, Q. Song, J. Zhuang and X. Ning, First-principles study of gas adsorption on c -graphyne, *Chem. Phys. Lett.*, 2017, **689**, 185–189.
 - 42 S. Kim and J. Y. Lee, Journal of Colloid and Interface Science Doping and vacancy effects of graphyne on SO 2 adsorption, *J. Colloid Interface Sci.*, 2017, **493**, 123–129.

- 43 X. Zhang, R. Fang, D. Chen and G. Zhang, Using Pd-Doped γ -Graphyne to Detect Dissolved Gases in Transformer Oil : A Density Functional Theory Investigation, *Nanomaterials*, 2019, **9**, 1490.
- 44 R. Majidi and M. Nadafan, diagnosis of lung cancer : A density functional theory study, *Phys. Lett. A*, 2020, **384**, 126036.
- 45 Y. Yao, Z. Jin, Y. Chen, Z. Gao, J. Yan, H. Liu, J. Wang, Y. Li and S. Frank, performance hydrogen evolution reaction, *Carbon N. Y.*, 2018, **129**, 228–235.
- 46 H. J. Hwang, Y. Kwon and H. Lee, Thermodynamically Stable Calcium-Decorated Graphyne as a Hydrogen Storage Medium, *J. Phys. Chem. C*, 2012, **116**, 20220–20224.
- 47 Y. Guo, X. Lan, J. Cao, B. Xu, Y. Xia, J. Yin and Z. Liu, A comparative study of the reversible hydrogen storage behavior in several metal decorated graphyne, *Int. J. Hydrogen Energy*, 2013, **38**, 3987–3993.
- 48 Y. Guo, K. Jiang, B. Xu, Y. Xia, J. Yin and Z. Liu, Remarkable hydrogen storage capacity in Li-decorated graphyne: Theoretical predication, *J. Phys. Chem. C*, 2012, **116**, 13837–13841.
- 49 J. Drogar, M. R. Roknabadi, M. Behdani, M. Modarresi and A. Kari, Superlattices and Microstructures Hydrogen adsorption on the a -graphyne using ab initio calculations, *SUPERLATTICES Microstruct.*, 2014, **75**, 340–346.
- 50 M. Bartolomei, E. Carmona-Novillo and G. Giorgi, First principles investigation of hydrogen physical adsorption on graphynes' layers, *Carbon N. Y.*, 2015, **95**, 1076–1081.

- 51 N. Wang, X. Li, Z. Tu, F. Zhao, J. He, Z. Guan, C. Huang, Y. Yi and Y. Li, Synthesis and Electronic Structure of Boron-Graphdiyne with an sp-Hybridized Carbon Skeleton and Its Application in Sodium Storage, *Angew. Chemie - Int. Ed.*, 2018, **57**, 3968–3973.
- 52 W. Ding, M. Sun, B. Gao, W. Liu, Z. Ding and S. Anandan, A ball-milling synthesis of N-graphyne with controllable nitrogen doping sites for efficient electrocatalytic oxygen evolution and, 2020, 10958–10969.
- 53 R. Schlo, A. Thomas, A. Fischer, F. Goettmann, M. Antonietti, J. Mu and J. M. Carlsson, Graphitic carbon nitride materials : variation of structure and morphology and their use as metal-free catalysts, 2008, 4893–4908.
- 54 G. Algara-siller, N. Severin, S. Y. Chong, T. Björkman, R. G. Palgrave, A. Laybourn, M. Antonietti, Y. Z. Khimyak, A. V Krashennnikov, J. P. Rabe, U. Kaiser, A. I. Cooper, A. Thomas and M. J. Bojdys, Triazine-Based Graphitic Carbon Nitride : a Two- Dimensional Semiconductor **, 2014, 7450–7455.
- 55 J. Mahmood, E. K. Lee, M. Jung, D. Shin, I. Jeon, S. Jung, H. Choi, J. Seo, S. Bae, S. Sohn, N. Park, J. H. Oh, H. Shin and J. Baek, Nitrogenated holey two-dimensional structures, 2015, 4–10.
- 56 Y. N. Xu and W. Y. Ching, Calculation of ground-state and optical properties of boron nitrides in the hexagonal, cubic, and wurtzite structures, *Phys. Rev. B*, 1991, **44**, 7787–7798.
- 57 K. Watanabe, T. Taniguchi and H. Kanda, Direct-bandgap properties and evidence for ultraviolet lasing of hexagonal boron nitride single crystal, *Nat. Mater.*, 2004, **3**, 404–409.

- 58 N. Otero, P. Karamanis, K. E. El-Kelany, M. Rérat, L. Maschio, B. Civalieri and B. Kirtman, Exploring the linear optical properties of borazine (B₃N₃) doped graphenes. 0D flakes vs 2D sheets, *J. Phys. Chem. C*, 2017, **121**, 709–722.
- 59 P. Karamanis, N. Otero and C. Pouchan, Unleashing the quadratic nonlinear optical responses of graphene by confining white-graphene (h -BN) sections in its framework, *J. Am. Chem. Soc.*, 2014, **136**, 7464–7473.
- 60 Y. Lin, T. V Williams and J. W. Connell, Soluble, Exfoliated Hexagonal Boron Nitride Nanosheets, 2010, **2**, 277–283.
- 61 J. C. Phys, J. Zhou, K. Lv, Q. Wang, X. S. Chen, Q. Sun and P. Jena, Electronic structures and bonding of graphyne sheet and its BN analog, , DOI:10.1063/1.3583476.
- 62 Y. Sun, H. Bai and Y. Huang, RSC Advances Structures , electronic properties and charge carrier, 2015, 8965–8973.
- 63 I. Muhammad, Nanoscale graphdiyne : stability and properties †, 2019, 9000–9007.
- 64 X. Liu, S. M. Cho, E. H. Baek, D. Hyun, H. Lee, X. Liu, S. M. Cho, S. Lin, Z. Chen, W. Choi and Y. Kim, Article Constructing two-dimensional holey graphyne with unusual annulative p -extension Constructing two-dimensional holey graphyne with unusual annulative p -extension, *Matter*, 2022, **5**, 2306-2318.
- 65 Y. Gao, H. Zhang, H. Pan and Q. Li, Ultrahigh hydrogen storage capacity of holey graphyne, *Nanotechnology*, 2021, **32**, 215402.
- 66 V. Mahamiya, A. Shukla, N. Garg and B. Chakraborty, High-capacity reversible hydrogen storage in scandium decorated holey graphyne: Theoretical perspectives, *Int.*

J. Hydrogen Energy, 2022, **47**, 7870–7883.

- 67 G. Kresse and J. Furthmüller, Efficiency of ab-initio total energy calculations for metals and semiconductors using a plane-wave basis set, *Comput. Mater. Sci.*, **6**, 15-50.
- 68 G. Kresse and J. Hafner, Ab. initio molecular dynamics for liquid metals, *Phys. Rev. B*, 1993, **47**, 558.
- 69 G. Kresse and J. Hafner, Ab initio molecular-dynamics simulation of the liquid-metal-amorphous-semiconductor transition in germanium, *Phys. Rev. B*, 1994, **49**, 14251.
- 70 G. Kresse and J. Furthmüller, Efficient iterative schemes for ab initio total-energy calculations using a plane-wave basis set, *Phys. Rev. B*, 1996, **54**, 11169.
- 71 J. P. Perdew, K. Burke and M. Ernzerhof, Generalized gradient approximation made simple, *Phys. Rev. Lett.*, 1996, **77**, 3865–3868.
- 72 A. D. Becke and K. E. Edgecombe, A simple measure of electron localization in atomic and molecular systems, *J. Chem. Phys.*, 1990, **92**, 5397.
- 73 P. Carloni, U. Rothlisberger and M. Parrinello, The Role and Perspective of Ab Initio Molecular Dynamics in the Study of Biological Systems, *Acc. Chem. Res.*, 2002, **35**, 455-464.
- 74 A. M. Virshup, C. Punwong, T. V. Pogorelov, B. A. Lindquist, C. Ko, and T. J. Martínez, Photodynamics in Complex Environments: Ab Initio Multiple Spawning Quantum Mechanical/Molecular Mechanical Dynamics, *J. Phys. Chem. B*, 2009, **113**, 3280–3291
- 75 S. A. Hollingsworth and R. O. Dror, Molecular dynamics simulation for all, *Neuron*,

2018, **19**, 1129-1143.

- 76 Nosé S, A unified formulation of the constant temperature molecular dynamics methods, *J. Chem. Phys.*, 1984, **81** 511–519.
- 77 H. Shin, S. Kang, J. Koo, H. Lee, J. Kim and Y. Kwon, Cohesion energetics of carbon allotropes: Quantum Monte Carlo study, *J. Chem. Phys.*, 2014, **140**, 1–18.
- 78 S. Ahmad and S. Mukherjee, A Comparative Study of Electronic Properties of Bulk MoS₂ and Its Monolayer Using DFT Technique: Application of Mechanical Strain on MoS₂ Monolayer, *Graphene*, 2014, **03**, 52–59.
- 79 X. Liu¹, S. Lin, E. Yun and H. Lee, Direct Band Gap Semiconducting Holey Graphyne: Structure, Synthesis and Potential Applications, *Arxiv*.
<https://doi.org/10.48550/arXiv.1907.03534>
- 80 Y. Gao, H. Zhang, H. Pan, Q. Li and J. Zhao, Ultrahigh hydrogen storage capacity of holey graphyne, *Nanotechnology*, 2021, **32**, 215402.
- 81 P. Deák, B. Aradi, T. Frauenheim, E. Janzén and A. Gali, Accurate defect levels obtained from the HSE06 range-separated hybrid functional, *Phys. Rev. B - Condens. Matter Mater. Phys.*, 2010, **81**, 1–4.
- 82 J. Zhou, M. M. Wu, X. Zhou and Q. Sun, Tuning electronic and magnetic properties of graphene by surface modification, *Appl. Phys. Lett.*, 2009, **95**, 103108.
- 83 S. B. Pillai, B. A. Baraiya, D. Upadhyay, V. Mankad and P. K. Jha, Catalytic activity and underlying atomic rearrangement in monolayer CoOOH towards HER and OER, *Int. J. Hydrogen Energy*, 2020, **45**, 23900–23907.
- 84 D. Chodvadiya, P. K. Jha and B. Chakraborty, Theoretical inspection of Ni/ α -SiX

(X=N, P, As, Sb, Bi) Single-Atom catalyst: Ultra-high performance for hydrogen evolution reaction, *Int. J. Hydrogen Energy*, , DOI:10.1016/j.ijhydene.2022.02.159.

Supporting Information

Prediction of a Novel 2D Porous Boron Nitride Material with Excellent Electronic, Optical and Catalytic Properties

Vikram Mahamiya^a, Alok Shukla^{a}, and Brahmananda Chakraborty^{b,c}*

^aIndian Institute of Technology Bombay, Mumbai 400076, India

^bHigh pressure and Synchrotron Radiation Physics Division, Bhabha Atomic Research Centre, Bombay, Mumbai, India-40085

^cHomi Bhabha National Institute, Mumbai, India-400094

email: mahamiyavikram@gmail.com ; shukla@iitb.ac.in ; brahma@barc.gov.in

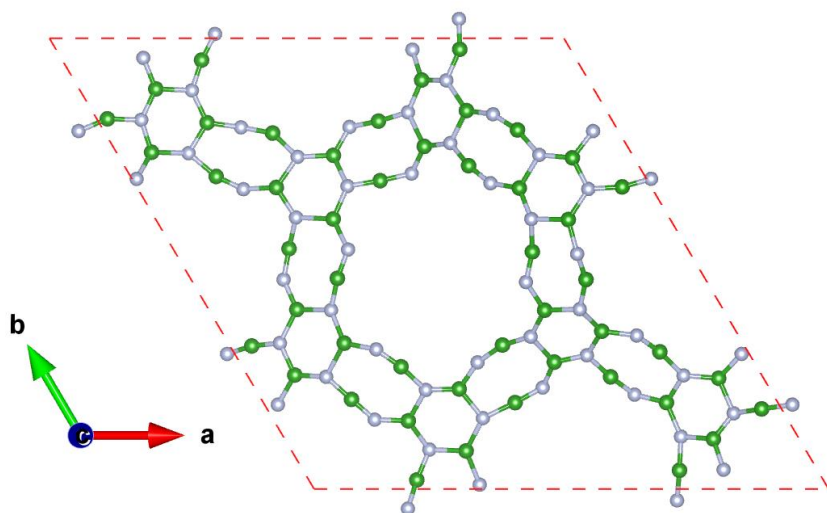


Fig. S1 Molecular dynamics snapshot of the monolayer BN-HGY after keeping the structure in a canonical ensemble for 5 ps time duration at 1000 K.

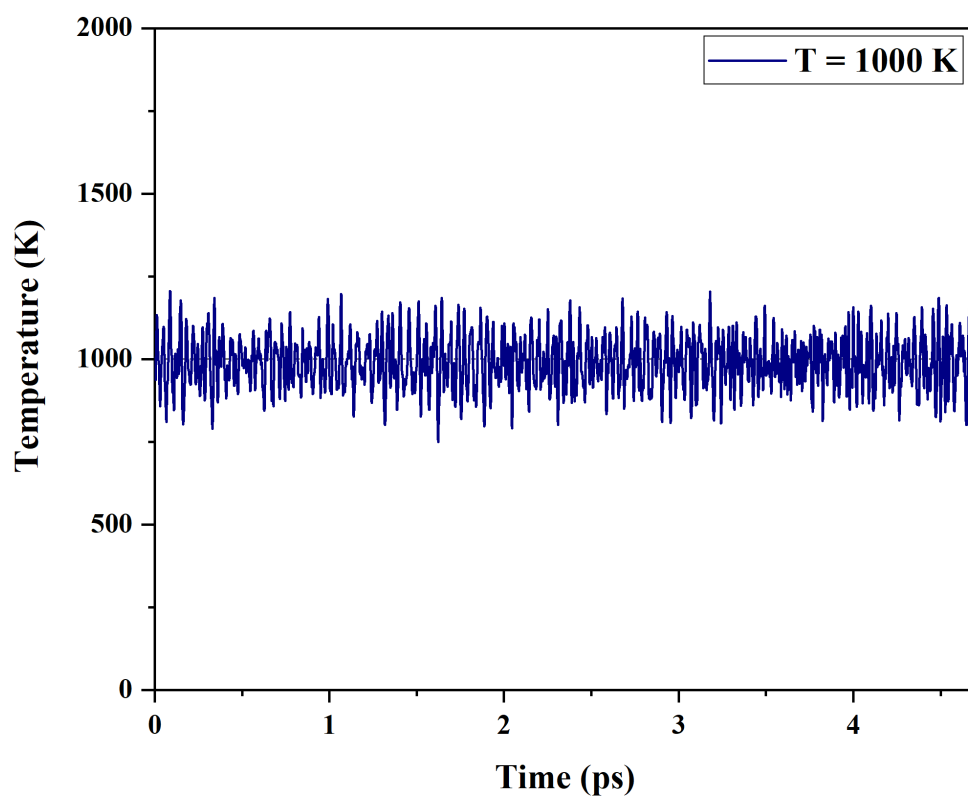


Fig. S2 Temperature fluctuations in the monolayer BN-HGY after keeping the structure in a canonical ensemble for 5 ps time duration at 1000 K.

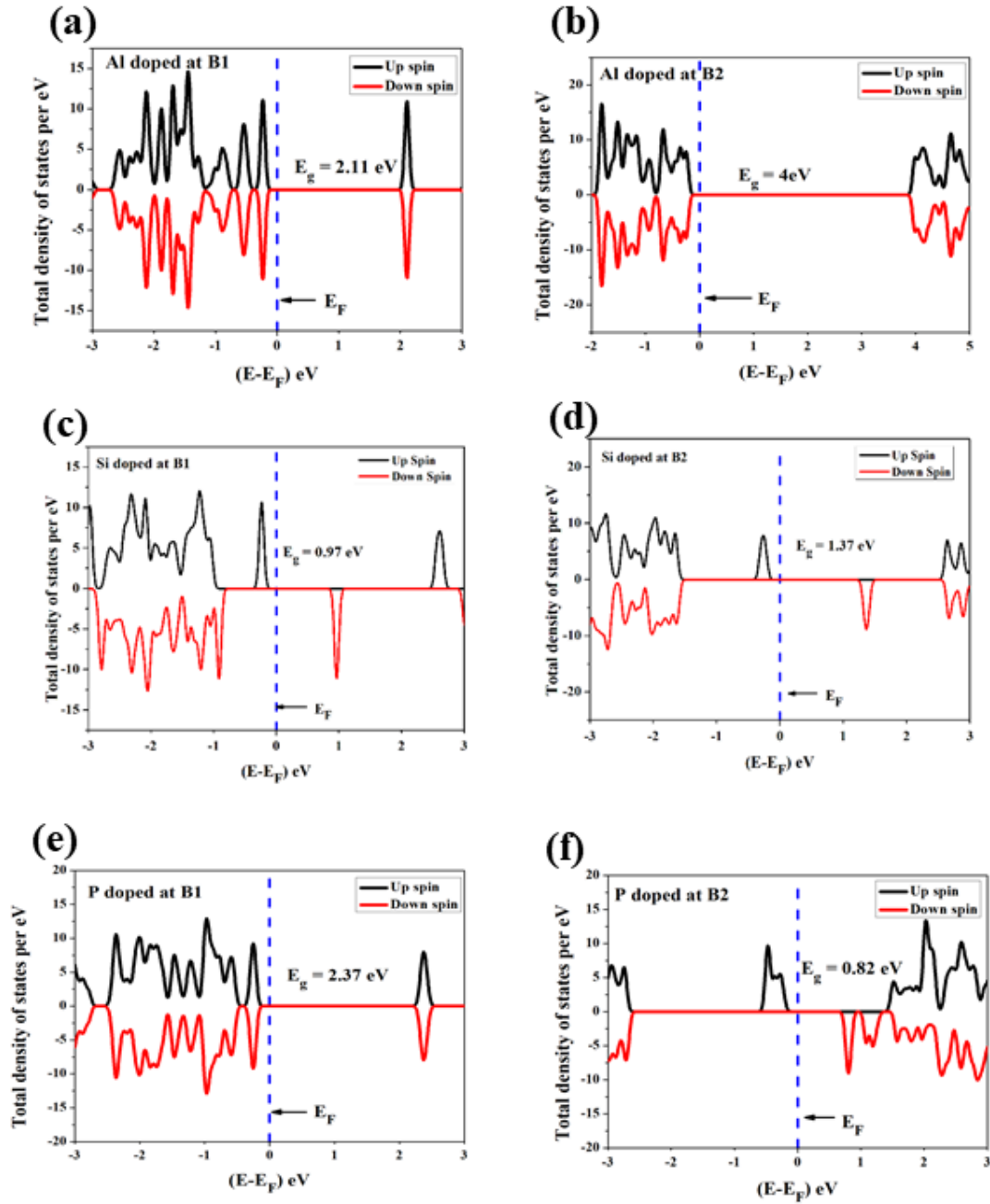


Fig. S3 Total density of states of BN-HGY with (a) Single aluminum atom doped at sp-hybridized boron atom (b) Single aluminum atom doped at sp^2 -hybridized boron atom (c) Single silicon atom doped at sp-hybridized boron atom (d) Single silicon atom doped at sp^2 -hybridized boron atom (e) Single phosphorus atom doped at sp-hybridized boron atom (f) Single phosphorus atom doped at sp^2 -hybridized boron atom. E_F represents the Fermi level.

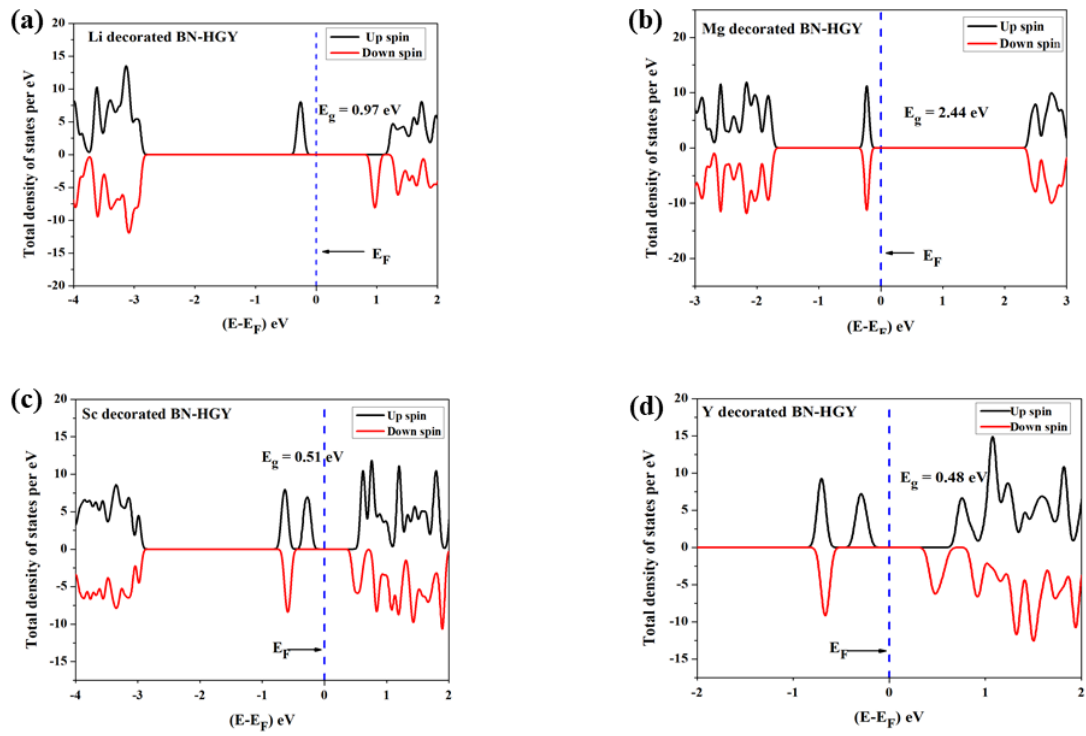


Fig. S4 Total density of states of (a) Li decorated BN-HGY (b) Mg-decorated BN-HGY (c) Sc-decorated BN-HGY (d) Y-decorated BN-HGY. E_F denotes Fermi energy.

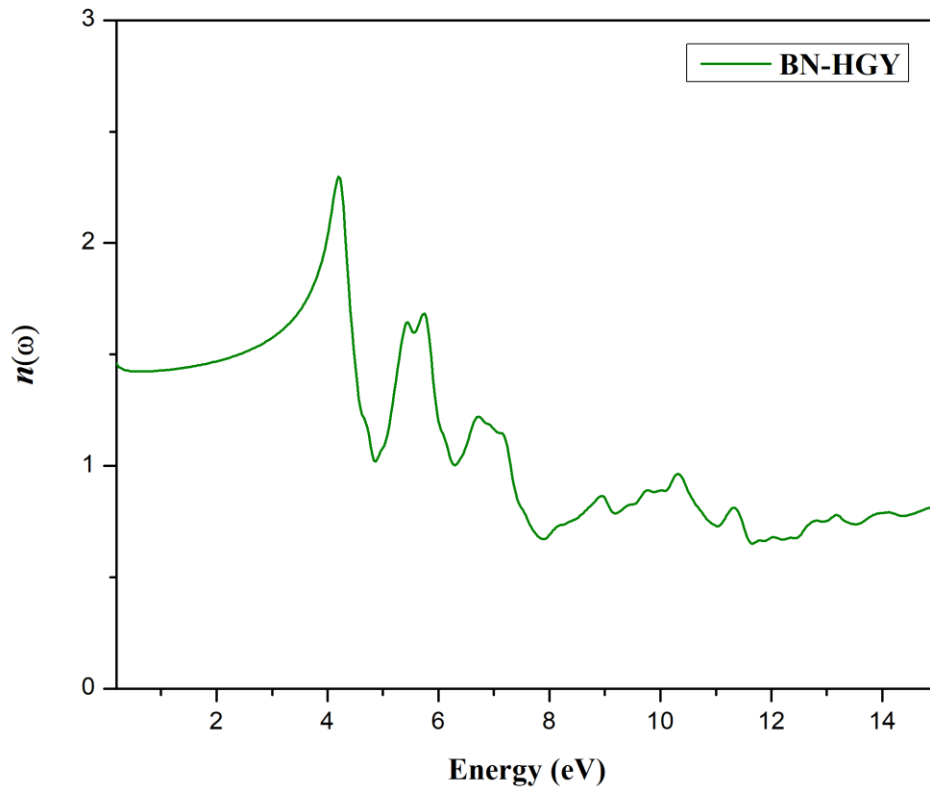


Fig. S5 The refractive index plot of the BN-HGY structure with respect to the energy of incident photon.

Structural files:

1. Position of atoms in BN-HGY unit cell

BN-HGY

1.0000000000000000

10.9187088012999993 0.0000000000000000 0.0000000000000000

-5.4644601315000001 9.4615217934999993 0.0000000000000000

1.3044178647000000 0.7099982333000000 7.5775218135999998

B N

12 12

Direct

0.0566971741682597 0.6389019931994668 0.5018388516514525
0.1926874521823643 0.5241284730690586 0.5012197681296378
0.3218171424157124 0.7982716503003187 0.5016855801975619
0.4669220795893775 0.6691744218433832 0.5018387624006801
0.5725211902550887 0.9341637378051905 0.5019189730254173
0.3519706552889871 0.4184862157155985 0.5012359759626668
0.6353967778918047 0.5757821353811766 0.5022334759707305
0.5204436674834406 0.3250939335024693 0.5015809636535463
0.7947645531143873 0.4701586566270122 0.5016157812398711
0.6655779729666641 0.1960166681748829 0.5016103778809397
0.4147832580016411 0.0600643152078548 0.5018746838700133
0.9307550666637444 0.3553966042863624 0.5010272359740948
0.3226075156284158 0.9275871673930171 0.5018549750617227
0.1939316097735876 0.6610441430644834 0.5014884701381875
0.0632850876362697 0.3956218344595660 0.5009678428583562
0.4575531243243695 0.7970143007302519 0.5017688523523787
0.3300044546311929 0.5335609467509147 0.5011614047239463
0.3919623584420341 0.3260800870234892 0.5013022215545587
0.5953149394131602 0.6681437310394783 0.5027267575151194
0.6574528424741708 0.4607432088436683 0.5017602759131905
0.5297974545867215 0.1972455870458008 0.5016512609867482
0.7935621599514922 0.3332835057476856 0.5011492330039808
0.6646755723940350 0.0666394356041891 0.5020633883436865
0.9241158907230623 0.5986472471846720 0.5021248875915024

2. BN-HGY (2*2 supercell) coordinates after keeping the system in canonical ensemble for 5 ps at 1000 K

BN-HGY

1.0000000000000000

21.8331655023710773 -0.0047829008094971 0.4308794721713001

-10.9265132170076207 18.9244222155918465 -0.0197986828702134

1.1546515469311316 0.6312696178755490 7.6087265711826575

B N

48 48

Direct

0.2036281492551567 0.0280764654485088 0.5710222100559605

0.2678061777307291 0.4643846405387267 0.6190915756682150

0.3050929325133986 0.2802539647389553 0.6109439486508895

0.1593161314111343 0.2034104530422128 0.6294810597982207

0.4601938521841759 0.1699757458804616 0.5871644829483099

0.0120527634950182 0.3207585580176112 0.5451805408171497

0.0779108853492657 0.2655464486561769 0.6175311741872769

0.3998220157295607 0.2337576299447987 0.6082082295976003

0.2171669001141310 0.3288617985019516 0.6211106889710546

0.2464222545365977 0.1593845209284770 0.6088194660204741

0.1439034117663819 0.3988898743237075 0.6343725685998401

0.3267680840811488 0.0899948261509044 0.5984998634633708

0.7166385103849671 0.0303083269181663 0.3885215117849110

0.7910841738411020 0.4566833139316616 0.4373179960059701

0.8105390596525683 0.2826980347021949 0.4124203619663437

0.6773419015502127 0.2076077775290202 0.4228284503828545

0.9563639452784801 0.1822345783922670 0.5333618461010741
0.5369227819712191 0.3259767688038166 0.5080955701484026
0.5935168386436719 0.2610353533244100 0.4899391430391826
0.8836183682436183 0.2324242740242426 0.5019601770464384
0.7334086942150361 0.3329624053219402 0.4163936018948027
0.7540137216275319 0.1588636390854377 0.4415285542885732
0.6700803072694629 0.4040265673451561 0.4266473233462995
0.8283295340615343 0.0973745342867041 0.4821222599525817
0.1993160619447869 0.5366471748893612 0.5965399197919804
0.2818007919881005 0.9690326093352192 0.5236486860985999
0.3379264833966513 0.7980946130787244 0.4718321772605788
0.1806219789210946 0.7133700955443698 0.4889208536587170
0.4678930938348433 0.6843672120911711 0.4860767644415845
0.0261931503448799 0.8196054729276446 0.5132817118855684
0.1031525182473200 0.7727910104485824 0.5238412446345054
0.4026791851676162 0.7339669915735516 0.5004788752570800
0.2425357693111955 0.8405513129005128 0.4698954114118827
0.2702225984302101 0.6668874055367587 0.5195672250911293
0.1617921287580946 0.9019915949527576 0.5223868605061228
0.3318491250544859 0.5947782095120985 0.5369980703645492
0.7211010632045479 0.5309377903719137 0.3868169994027751
0.7959184592642345 0.9677532589246399 0.4011122644955291
0.8153038978060662 0.7796054386777722 0.4999613794502541
0.7023844501296874 0.7223119957831291 0.4007379470945192
0.9698856280704190 0.6795294244330000 0.5233612824391263
0.5385562277904894 0.8195846490456975 0.4070311773929284
0.6056450004361985 0.7653443190382317 0.4116162431847509

0.9017304695747720 0.7304829373608045 0.5062550811679223
0.7417404683796663 0.8383660806204103 0.4077831624862359
0.7658991319478162 0.6634139814078596 0.4538821936948894
0.6802002112201766 0.9087430610377327 0.3506472512050274
0.8383697091033305 0.5947159541810579 0.4684711236184836
0.0153956097870634 0.1974676057651645 0.5947576624195341
0.4686583988698264 0.2971631219919850 0.5517869623349980
0.2820900497344097 0.3257419007238896 0.6103051647655964
0.1889093200137907 0.1650709332407357 0.6297515273231397
0.1474396258042908 0.4694400351645467 0.6328796622634102
0.3257656988528185 0.0285587711800658 0.5677925410850810
0.2631300448750821 0.0983484378263844 0.5846115743174616
0.2143805592776156 0.3932987063460976 0.6284915977622849
0.3195646972707713 0.2244333409886548 0.5984701707543658
0.1423189329494558 0.2604139244196826 0.6380410210483887
0.3910529921990516 0.1552382064059745 0.6214498414901723
0.0814217447813934 0.3339036297553277 0.5875900042216677
0.5272241856938954 0.2011426480365264 0.5331527857159237
0.9411043148225871 0.2961918429108191 0.5598022359974238
0.8004211439934038 0.3385184302155906 0.4116450248433894
0.6864404181515941 0.1498027394921835 0.4143850062697798
0.6714498967636030 0.4669204382384811 0.3716429886812222
0.8324527489103654 0.0316606901442585 0.4332302476433474
0.7602801096162659 0.0933050171181440 0.4502740378242267
0.7345144911888531 0.3957650748094211 0.4042882269277618
0.8200513380774878 0.2258565147317521 0.4519035572528164
0.6669411832989535 0.2654846919305127 0.4490628660357877

0.8912937774837462 0.1661946483040107 0.4928303826769458
0.6059714785478597 0.3324662373282478 0.4555714297875061
0.0364542107150111 0.7091816637653520 0.5419229739128160
0.4716724720907199 0.7968039800097688 0.4873620884997042
0.3090749447115717 0.8388846087615381 0.4638091743327756
0.2163012328560122 0.6833068044031865 0.5031500889918384
0.1565279226595129 0.9639938516675695 0.5511525787796777
0.3276543182865906 0.5291712604957809 0.5580072114576948
0.2657780890316491 0.6008311579280678 0.5486610028869615
0.2312839662724321 0.9024749858968487 0.4798126677367953
0.3358159140402322 0.7364625145955531 0.5230261165617168
0.1722420740279486 0.7752418621797524 0.4718732742199275
0.3968312390887554 0.6651897036440303 0.5143875424483740
0.0976881362015598 0.8339424683567281 0.5248343746788446
0.5333539356731349 0.6994729611661658 0.4541491415263179
0.9592877294838226 0.7991912819069537 0.5037539231845954
0.7961457605525440 0.8261293558057264 0.4760753657337705
0.7154627528770752 0.6702389603460113 0.3804331732098948
0.6791645559650548 0.9676730653592902 0.3465987577570060
0.8261565676640602 0.5243414021486195 0.4535701213994284
0.7729699326212152 0.5946550314653117 0.4289543561955404
0.7491959258869550 0.9062434239060168 0.3607290026739423
0.8322263371987463 0.7233107100235863 0.5048168681136913
0.6806307651236162 0.7689013858097599 0.3617915266578634
0.9014567151302696 0.6607245912577789 0.5039292193314608
0.6099451668070720 0.8328739215196856 0.3602942163631202